Pronounced enhancement of thermal expansion coefficients of rare-earth zirconate by cerium doping

Yang, Jun; Zhao, Meng; Zhang, Lei; Wang, Ziyuan; Pan, Wei

Regular article

Pronounced enhancement of thermal expansion coefficients of rare-earth zirconate by cerium doping

Jun Yang [a], Meng Zhao [b], Lei Zhang [c], Ziyuan Wang [a], Wei Pan [a,*]

[a] State Key Laboratory of New Ceramics and Fine Processing, Department of Materials Science and Engineering, Tsinghua University, Beijing 100084, PR China
[b] Department of Material Science and Engineering, Delft University of Technology, The Netherlands
[c] Department of Electrical and Electronic Engineering, Southern University of Science and Technology, Shenzhen 518055, PR China

ABSTRACT

Rare-earth zirconates ($RE_2Zr_2O_7$, RE = rare earth elements) are considered as promising thermal barrier coating (TBCs) materials. However, their thermal expansion coefficient (TEC) is relatively low comparing with that of either the state-of-the-art TBCs material Yttria-stabilized Zirconia (YSZ), or the metallic bond-coat. In present research, Cerium was introduced as the substitution of Zirconium to improve the TEC of rare-earth zirconates. A series of $Yb_2(Zr_{1-x}Ce_x)_2O_7$ solid solutions were synthesized and investigated. Experimental results revealed that their TEC is remarkably increased with the Cerium substitution content. Meanwhile, their thermal conductivity shows no obvious increase compared with that of $Yb_2Zr_2O_7$ due to the phonon scattering effect.

© 2018 Acta Materialia Inc. Published by Elsevier Ltd. All rights reserved.

Thermal barrier coatings (TBCs) are commonly employed in hot-path components in gas turbines, jet engines and other propulsion systems to protect the super-alloy components, hence enable the engines to operate at higher temperatures [1–9]. The state-of-the-art TBCs materials is 7–8 wt% Yttria-stabilized Zirconia (YSZ) with relatively low thermal conductivity and good comprehensive mechanical properties [1,5–7]. However, there are still some problems, such as the non-equilibrium phase degradation, silicate melts generically known as CMAS corrosion, thermally grown oxides, restricting the further application of YSZ above 1200 °C [1–3,5]. In the past decade, an enhanced investigation of novel materials has led to the discovery of some promising candidates for TBCs at higher temperatures [4–6]. Among them, $RE_2Zr_2O_7$-type rare-earth zirconates with pyrochlore or defective fluorite structure are proposed as practical alternatives of YSZ and have already been applied in some high temperature gas turbines [7]. However, the relatively low thermal expansion coefficient (TEC) is the fatal problem of the rare-earth zirconates to be improved [5,6].

In present research, a series of $Yb_2(Zr_{1-x}Ce_x)_2O_7$ compounds are designed and investigated, in consideration that the lattice relaxation induced by the substitutions may increase the TEC, while the phonon scattering effect may also reduce the thermal conductivity. The $Yb_2(Zr_{1-x}Ce_x)_2O_7$ (x = 0, 0.1, 0.3, 0.5) specimens were synthesized by the solid-state reaction method. The starting materials were Yb_2O_3 (99.99%, Rare-Chem. Hi-Tech. Co., Ltd), ZrO_2 (99.9%, Guangdong Orient Zirconic Ind. Sci & Tech Co., Ltd), CeO_2 (>99.5%, Tianjin Bodi Chemical Industry Co. Ltd), which were precisely weighted to yield the designed compositions and ball-milled with ethanol by a planetary-mill (Fritsch, Pulverisette 6) for 12 h (300 r/min). Notably, all starting materials were calcined at 1000 °C for 5 h before weighting to remove the gas absorptions. The slurries were rotary evaporated and dried at 120 °C for 24 h to complete the dehydration. The resulting powders were sieved and pressed by uniaxial cold pressing (100 MPa) followed by isotactic cold pressing (220 MPa, 5 min) to prepare the green bodies with proper shapes and sizes. Then the green bodies were pressure-less sintered to obtain the dense specimens. The sintering process, relative density and phase structure of the specimens are shown in Table 1. The relative density of all the specimens measured by the Archimedes method is higher than 95%. Finally, the specimens were machined into 1 mm × Φ10mm discs and 4.5 × 4 × 25 mm cuboids for thermal conductivity and TEC measurements, respectively.

The phase structure of the specimens was characterized by X-ray diffraction (XRD, D/max-RB, Rigaku, Japan, Cu/Kα) at a scanning speed of 10°/min and their microstructure was observed by scanning electron microscopy (SEM, JSM-7001F, JEOL, Japan). Raman spectroscopy (LabRAM HR800, Horiba, France, He—Ne laser with radiation at 632.81 nm) was applied to estimate the detailed lattice structure of the specimens, as a complement of the XRD results. The accuracy of the recording of wave numbers is about 1 cm^{-1}. Thermal diffusivity (α) of the specimens was measured by the laser flash method (Netzsch

Table 1
The phase content, sintering process, relative density and phase structure of $Yb_2(Zr_{1-x}Ce_x)_2O_7$ specimens.

x	Composition	Abbreviation	Sintering process	Relative density	Phase[a]
0	$Yb_2Zr_2O_7$	YZ	1600 °C/10 h	>99%	F
0.1	$Yb_2(Zr_{0.9}Ce_{0.1})_2O_7$	YZ9C1	1600 °C/10 h	95.1%	F
0.3	$Yb_2(Zr_{0.7}Ce_{0.3})_2O_7$	YZ7C3	1600 °C/10 h	95.8%	F
0.5	$Yb_2(Zr_{0.5}Ce_{0.5})_2O_7$	YZ5C5	1550 °C/5 h	96.1%	F

[a] F represents the fluorite structure phase.

LFA 427, Bavaria, Germany) from room temperature (RT) to 1000 °C in an argon atmosphere and the results were corrected by Cape-Lehmann model [10]. Thermal conductivity (κ_0) was then calculated as

$$\kappa_0 = \rho \cdot c \cdot \alpha \tag{1}$$

where c is the heat capacity estimated by Neumann–Kopp rule and ρ is the bulk density of the specimens. Taking into account of the porosity (ϕ), thermal conductivity (κ) of fully dense specimens can be modified as [11].

$$\kappa_0/\kappa = 1 - 4/3\phi \tag{2}$$

Besides, TEC was measured by thermal expansion instrument (NETZSCH, DIL 402HP) within the temperature range of RT to 1500 °C.

As shown in Fig.1(a), all the specimens exhibit a fluorite phase structure (F-type) and no diffraction peaks of impurity phases were observed, indicating that all the starting materials have completely formed the solid solutions. The partial enlarged part of XRD patterns in Fig.1(b) reveals that the peaks shift to the lower angle with increasing fraction of Ce^{4+} due to its larger ionic radius comparing with Zr^{4+}. The

lattice parameters of substituted compounds increase linearly with composition (Fig.1(c)), which is in agreement with Vegard's law. Therefore, it can be concluded than Ce^{4+} has entered the site of Zr^{4+} and infinite substitutional solid solutions have formed. Raman spectroscopy, which is primarily sensitive to the short-range periodicity, was applied to explore the lattice structure of the specimens and the results gives a further insight. As shown in Fig.1(d), YZ specimen has almost no Raman activity due to the disorder of its defective fluorite structure. However, with the increase of the Ce^{4+} fraction, Raman intensity of the specimens shows a gradual increase. It was reported that the Raman activity of solid solutions increases due to the super-lattice structure (C-type) introduced by the Ce^{4+} substitution [12]. In brief, all the substituted specimens show a defective fluorite-type structure, yet as the Ce^{4+} fraction increases, the ordering of the lattice is enhanced. Furthermore, according to SEM images of the specimens shown in Fig.2, the grain boundaries are clean and clear, no intermediate phases or precipitated particles were observed, indicating the single phase structure and the good stability of the specimens at sintering temperature.

It is widely accepted that the failure of TBCs is mainly caused by the TEC mismatch between top-coat, TGO and bond-coat, as well as the related thermal stress accumulation [1–3]. Thus, relatively high TEC is of
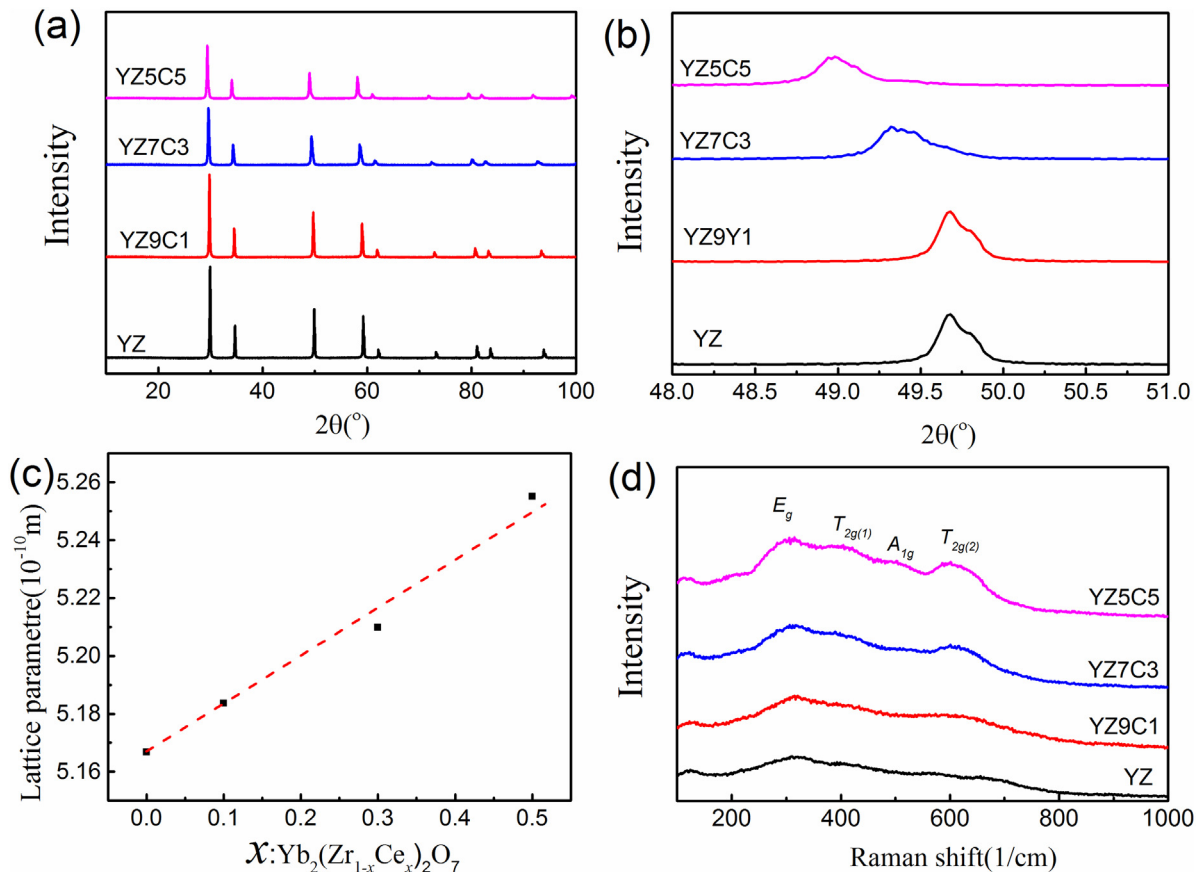

Fig. 1. Structural characterization of specimens (a) XRD patterns, (b) Partial enlarged detail of XRD patterns, (c) Lattice parameters, (d) Raman spectrum.
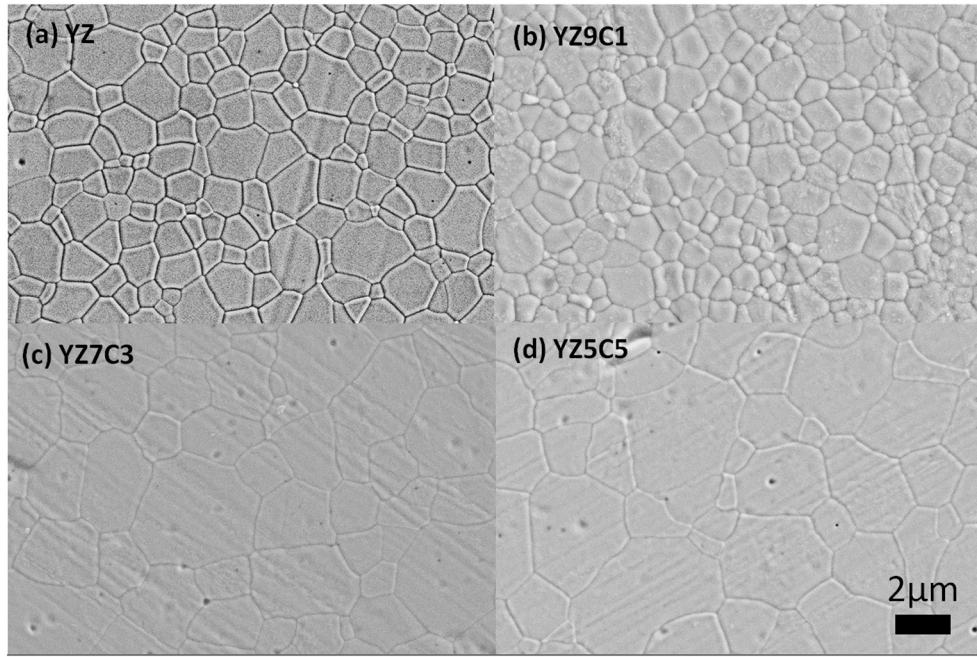
Fig. 2. SEM micrographs of hot corrosion surface of specimens (a)YZ, (b)YZ9C1, (c)YZ7C3, (d)YZ5C5.

great importance to improve the lifetime of TBCs. Fig.3(a) shows the temperature dependence of the thermal expansion rate $\Delta L/L_0$ of Yb_2 $(Zr_{1-x}Ce_x)_2O_7$ specimens within the range from RT to1500 °C. Several conclusions can be obtained: (i) the thermal expansion curve of all the specimens keep a linear relation, indicating no phase transition occurs over the temperature range; (ii) the expansion rates of the substituted specimens are greater than that of $Yb_2Zr_2O_7$; (iii) the higher fraction of Ce substitution, the higher the thermal expansion rate. This can also be seen more clearly in Fig.3(b) that the TEC increases rapidly with the increasing Ce fraction x. Furthermore, the inset figure of Fig.3 (b) shows that the engineering TEC (ETEC) of $Yb_2(Zr_{1-x}Ce_x)_2O_7$ has an approximately linearly increasing relation with x. There are many factors that influence the TEC of ceramic materials, and dominant factors are different for different materials. In present research, the improved TEC of $Yb_2(Zr_{1-x}Ce_x)_2O_7$ compounds can be attributed to several factors as follows: (i) lattice relaxation and distortion caused by the larger ionic size of Ce^{4+} substitutions than the Zr^{4+} matrix (as shown in Table 2); (ii) partial reduction of Ce^{4+} to Ce^{3+} at elevated temperatures [13];

(iii) weakened binding energy. It is known that, for ionic compounds, the crystal lattice energy can be expressed as [14]:

$$U = \frac{N_0 A z^+ z^- e^2}{r_0}\left(1 - \frac{1}{n}\right)$$ (3)

where N_0, A, z, r_0 and n represent the Avogadro's number, Madelung constant, ionic charge, inter-ionic distance, unit charge of electron and Born exponent, respectively. Considering the substituted compounds are all isostructural, it is reasonable to assume the Madelung constant and the Born exponent to be invariable. Hence, the lattice energy is mainly dominated by the inter-ionic distance. As shown in Fig.1(c), with an increasing x, the lattice parameter increases, which means an increasing of the r_0. Therefore, the lattice energy decreases with an increasing x, leading to a rise of the TEC.

Need to be further mentioned, as shown in Fig.3(b), the TEC has a sudden drop at about 200 °C for YZ7C3 and YZ5C5 specimens. A similar phenomena has also been reported for $La_2Ce_2O_7$ [13]. However, CeO_2
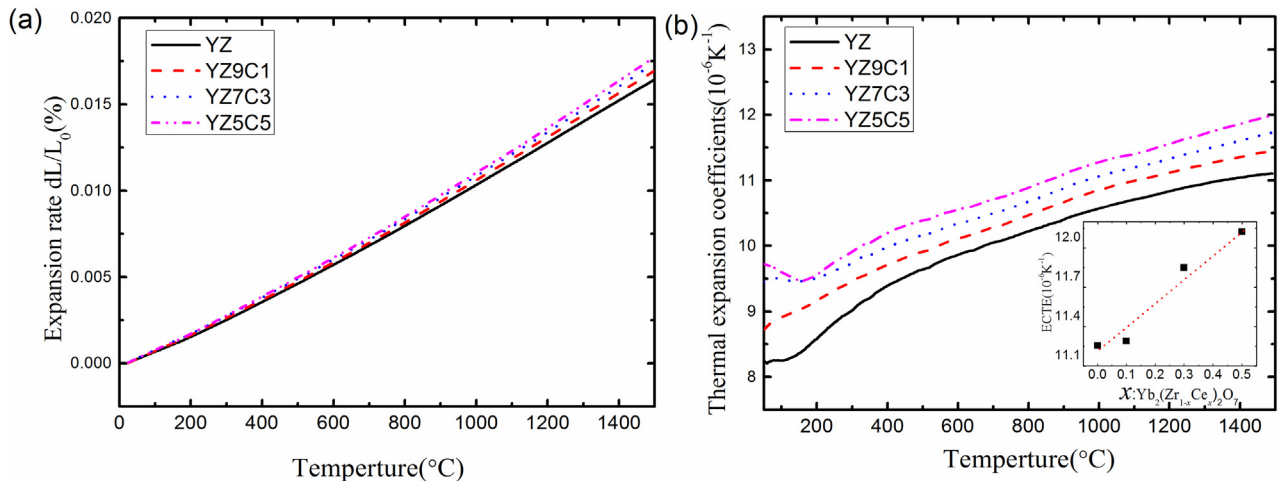

Fig. 3. Thermal expansion performance of specimens (a)Expansion rate, (b)Thermal expansion coefficients.

Table 2
The atomic mass and ionic radius of the relevant elements in the present research. For oxygen vacancies, they are assumed to be zero for simplicity.

Element	Zr^{4+}	Ce^{4+}	O^{2-}	□
Atomic mass (g/mol)	91.2	140.1	16.0	0
Ionic radius (pm)	72	87	137	0

does not have such a property. By XRD tests at elevated temperatures, it was shown that $La_2Ce_2O_7$ maintains the fluorite structure within 25–300 °C, but the lattice parameter contracts at about 190 °C [13]. As a comparison, the lattice parameter of $La_2Zr_2O_7$ shows monotonic increase with the increasing temperature. Considering there are a large number of oxygen vacancies and both the strength of vibration and the transverse vibration motions control the thermal expansion of the $La_2Ce_2O_7$, Cao et al. [13] attributed the thermal contraction of $La_2Ce_2O_7$ to the reason that transverse motion is comparable to the strength of vibration or even stronger than strength of vibration at the medium temperature in crystal.

Thermal conductivity is another key property of TBCs dominating the heat insulation ability. Reducing the intrinsic thermal conductivity is a major topic for developing advanced TBCs [15–21]. As shown in Fig.4(a), with Ce fraction increase, the thermal conductivity of $Yb_2(Zr_{1-x}Ce_x)_2O_7$ solid solutions decreased first and then increased. The increased phonon scattering due to the substitutions is considered to be mainly responsible for the thermal conductivity reduction [7]. Based on elastic continuum treatments, the theoretical thermal conductivity of the substituted compounds can be estimated [19]. The thermal conductivity of $Yb_2(Zr_{1-x}Ce_x)_2O_7$ compounds at temperatures above the Debye temperature is inversely proportional to the square root of the defect phonon scattering coefficient [22]:

$$\kappa \propto \Gamma^{-1/2} \tag{4}$$

For $A_2B_2O_7$ fluorite-related compounds, taking oxygen vacancies as imperfections on the O site, the scattering coefficient of solid solution is the integration of the scattering coefficient on A, B and O sites:

$$\Gamma = \frac{1}{6}\left(\frac{M_A}{\overline{M}}\right)^2 \Gamma_A + \frac{1}{6}\left(\frac{M_B}{\overline{M}}\right)^2 \Gamma_B + \frac{2}{3}\left(\frac{M_O}{\overline{M}}\right)^2 \Gamma_O \tag{5}$$

where $\overline{M}$ is the average atomic mass of the whole lattice. M_i and Γ_i refer to the average atomic mass and scattering coefficient on the corresponding site, respectively. Specifically for $Yb_2(Zr_{1-x}Ce_x)_2O_7$ solid

solutions, and the scattering coefficient on each site can be written as ($\Gamma_A = 0$):

$$\Gamma_B = x(1-x)\left[\left(\frac{\Delta M_B}{M_B}\right)^2 + \varepsilon\left(\frac{\Delta\delta_B}{\delta_B}\right)^2\right] \tag{6}$$

$$\Gamma_O = \frac{1}{8} \times \frac{7}{8}\left[\left(\frac{\Delta M_O}{M_O}\right)^2 + \varepsilon\left(\frac{\Delta\delta_O}{\delta_O}\right)^2\right] \tag{7}$$

where δ_i is the average ionic radius on the corresponding site, and ε the strain field factor which can be expressed by the Grüneisen parameter γ and Poisson ratio σ:

$$\varepsilon = \frac{2}{9}\left(6.4 \times \gamma \times \frac{1+\sigma}{1-\sigma}\right)^2 \tag{8}$$

$$\gamma = \frac{3\alpha_l K_T}{\rho C_p} \tag{9}$$

where α_l, K_T, ρ and C_p represent the TEC, isothermal bulk modulus, density and heat capacity, respectively. Using the atomic mass and ionic radius of the related elements as shown in Table 2, calculated results are shown in Fig.4(b) to compare with the experimental values at room temperature. One can see that, a comparison of the observed values with calculated values of the thermal conductivities showed a relatively good agreement, whereas the deviation becomes more and more obvious as doping concentration increased. The thermal conductivity of experimental values higher than the calculated results at high doping concentration mainly due to rare-earth zirconate cannot be seen as a matrix material at high doping concentration, and the $RE_2Ce_2O_7$ have higher thermal conductivity than that of $RE_2Zr_2O_7$. Furthermore, as mentioned above, the enhanced ordering of the lattice as Ce^{4+} fraction increases also give rise to the reduction of scattering coefficient, leading to the increase of thermal conductivity. However, as shown in Fig.4, the thermal conductivity of all substituted compounds have no obvious increased compared with the pure $Yb_2Zr_2O_7$ and lower than established YSZ.

In conclusion, a series of substituted compounds $Yb_2(Zr_{1-x}Ce_x)_2O_7$ ($x = 0, 0.1, 0.3, 0.5$) were synthesized and investigated. Due to the lattice relaxation and the conversion of Ce^{4+} to Ce^{3+} at elevated temperatures, the TEC of these solid solutions is remarkably increased. The engineering TEC has an approximately linear increase with the fraction of Ce substitution. It is also shown that, due to the strong phonon
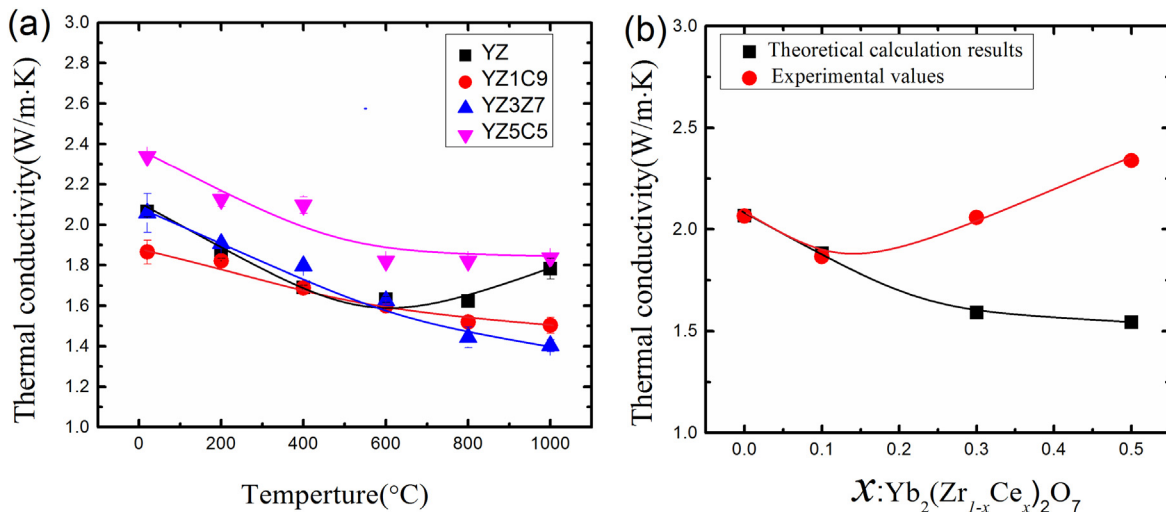

Fig. 4. Thermal conductivity of specimens (a) Experimental values, (b)Simulation results combing with experimental values at room temperature.

scattering, the thermal conductivity of solid solutions decreased at low doping concentration, and turn to almost stable at high doping concentration. The thermal conductivity is similar with $Yb_2Zr_2O_7$ and much lower than that of YSZ. Considering the stable phase structure, improved thermal expansion behavior and also the low thermal conductivity, $Yb_2(Zr_{1-x}Ce_x)_2O_7$ ($x \leq 0.5$) compounds may be promising candidates for thermal barrier coatings.

Acknowledgment

References

[1] N.P. Padture, M. Gell, E.H. Jordan, Science 296 (2002) 280–284.
[2] D.L. Poerschke, R.W. Jackson, C.G. Levi, Annu. Rev. Mater. Res. 47 (2017) 297–330.
[3] D.R. Clarke, C.G. Levi, Annu. Rev. Mater. Res. 33 (2003) 383–417.
[4] R. Vaßen, M.O. Jarligo, T. Steinke, D.E. Mack, D. Stöver, Surf. Coat. Technol. 205 (2010) 938–942.
[5] C.G. Levi, J.W. Hutchinson, M. Vidal-Sétif, C.A. Johnson, MRS Bull. 37 (2012) 932–941.
[6] N.P. Padture, Nat. Mater. 15 (2016) 804–809.
[7] M. Zhao, W. Pan, C. Wan, Z. Qu, Z. Li, J. Yang, J. Eur. Ceram. Soc. 37 (2017) 1–13.
[8] S. Sampath, U. Schulz, M.O. Jarligo, S. Kuroda, MRS Bull. 37 (2012) 903–910.
[9] R. Vaßen, Y. Kagawa, R. Subramanian, P. Zombo, D. Zhu, MRS Bull. 37 (2012) 911–916.
[10] J.A. Cape, G.W. Lehman, J. Appl. Phys. 34 (1963) 1909–1913.
[11] S.K. W, P.N. P, K.P. G, J, Mater. Sci. 36 (2001) 3003–3010.
[12] H. Yamamura, H. Nishino, K. Kakinuma, K. Nomura, J. Jan. Ceram. Soc. 111 (2003) 902–906.
[13] X. Cao, R. Vassen, W. Fischer, F. Tietz, W. Jungen, D. Stöver, P. Abrman, Adv. Mater. 15 (2003) 1438–1442.
[14] C. Wan, Z. Qu, A. Du, W. Pan, Acta Mater. 57 (2009) 4782–4789.
[15] J. Yang, C. Wan, M. Zhao, M. Shahid, W. Pan, J. Eur. Ceram. Soc. 36 (2016) 3809–3814.
[16] J. Yang, Y. Han, M. Shahid, W. Pan, M. Zhao, W. Wu, C. Wan, Scripta Mater. 149 (2018) 49–52.
[17] L. Chen, Y. Jiang, X. Chong, J. Feng, J. Am. Ceram. Soc. 101 (2018) 1266–1278.
[18] C.L. Wan, W. Pan, Q. Xu, Y.X. Qin, J.D. Wang, Z.X. Qu, M.H. Fang, Phys. Rev. B 74 (2006) 144109.
[19] J. Yang, M. Shahid, C. Wan, F. Jing, W. Pan, J. Eur. Ceram. Soc. 37 (2017) 689–695.
[20] C. Zhang, Y. Pei, L. Zhao, D. Berardan, N. Dragoe, S. Gong, H. Guo, J. Eur. Ceram. Soc. 34 (2014) 63–68.
[21] C. Wan, Z. Qu, Y. He, D. Luan, W. Pan, Phys. Rev. Lett. 101 (2008) 85901.
[22] M. Zhao, X. Ren, W. Pan, J. Am. Ceram. Soc. 98 (2015) 229–235.